JOURNAL OF AIRCRAFT
Vol. 42, No. 1, January–February 2005

Performance and Stability of a Winged Vehicle in Ground Effect

Nicola de Divitiis*
University of Rome "La Sapienza," 00184 Rome, Italy

The present work deals with the dynamics of vehicles that intentionally operate in the ground proximity. The dynamics in ground effect is influenced by the vehicle orientation with respect to the ground because the aerodynamic force and moment coefficients, which in turn depend on height and angle of attack, also vary with the Euler angles. This feature, usually neglected in the applications, can be responsible for sizable variations of the aircraft performance and stability. A further effect, caused by the sink rate, determines the unsteadiness that modifies the aerodynamic coefficients. In this work, an analytical formulation is proposed for the force and moment calculation in the presence of the ground and taking the aircraft attitude and sink rate into account. The aerodynamic coefficients are first calculated for a representative vehicle, and its characteristics in ground effect are investigated. Performance and stability characteristics are then discussed with reference to significant equilibrium conditions, while the nonlinear dynamics is studied through the numerical integration of the equations of motion.

Nomenclature

AR	=	aspect ratio
b	=	wing span
C_D	=	drag coefficient
C_L	=	lift coefficient
C_l, C_m, C_n	=	aerodynamic moment coefficients in body axes
C_x, C_y, C_z	=	aerodynamic force coefficients in body axes
c	=	mean wing chord
$\boldsymbol{F}$	=	nonviscous aerodynamic force
$\boldsymbol{F}_v$	=	viscous aerodynamic force
$\boldsymbol{F}^e$	=	sum of the external forces
$\boldsymbol{g}$	=	gravity acceleration
$\boldsymbol{H}$	=	$((H_{ijl}))$ third-order apparent-mass tensor
h	=	height
h/c	=	dimensionless height
$\boldsymbol{J}$	=	inertia tensor
$\boldsymbol{L}$	=	transformation matrix from inertial to body frame
l	=	vehicle length
$\boldsymbol{M}$	=	$((M_{ij}))$ second-order apparent-mass tensor
m	=	vehicle mass
$\boldsymbol{n}$	=	local normal unit vector
$\boldsymbol{P}$	=	linear momentum of the airstream
$\hat{p}, \hat{q}, \hat{r}$	=	$pb/V, qc/V, rb/V$ dimensionless angular velocity components
$\boldsymbol{Q}$	=	aerodynamic moment with respect to c.g.
$\boldsymbol{Q}^e$	=	sum of the external moment with respect to the c.g.
$\boldsymbol{R}^{-1}$	=	transformation matrix from $\boldsymbol{\omega}$ to $\dot{\Phi}$
$\boldsymbol{r} \equiv (x, y, z)$	=	aircraft c.g. position in Earth axes
$\boldsymbol{r}_{\text{c.g.}}$	=	aircraft c.g. position in body axes
S	=	wing area
S_v	=	vehicle wetted surface
T	=	kinetic energy of the stream flow
$\boldsymbol{T}$	=	thrust force
V	=	velocity modulus
$\boldsymbol{v}$	=	(u, v, w) inertial velocity in body axes
W	=	weight
x, y, z	=	Earth-fixed coordinates
x_B, y_B, z_B	=	body axes coordinates
α, β	=	angle of attack and sideslip, respectively
γ	=	flight-path angle
$\delta_e, \delta_a, \delta_r$	=	elevator, ailerons and rudder angles, respectively
δ_T	=	$\Pi/\Pi_{\max}$ throttle level
$\partial\phi/\partial\boldsymbol{v}$	=	$(\partial\phi/\partial u, \partial\phi/\partial v, \partial\phi/\partial w)$ potential by unit velocity
ζ	=	turn rate
η	=	propeller efficiency
$\boldsymbol{\lambda}(\lambda_x, \lambda_y, \lambda_z) \equiv \boldsymbol{L}(0, 0, 1)^T$	=	ground normal unit vector in body axes
Π	=	engine power
ρ	=	air density
$\tau \equiv \sqrt{[1 + 4(h/c)^2]} - 2h/c$	=	ground effect perturbative parameter
ϕ	=	velocity potential
φ, ϑ, ψ	=	Euler angles
$\boldsymbol{\omega}$	=	(p, q, r)-angular velocity vector in body axes

Subscripts

a.c.	=	aerodynamic center
c.g.	=	center of gravity
0	=	value calculated at $\varphi = \vartheta = 0$
∞	=	value calculated out of ground effect

Received 29 August 2003; revision received 14 March 2004; accepted for publication 15 March 2004.

*Research Fellow, Department of Mechanics and Aeronautics, via Eudossiana, 18.

Introduction

AN important feature of ground effect is the influence of the attitude on the vehicle dynamics. This influence arises from the Euler angles, which has an effect on the aerodynamic force and moment coefficients. This is of paramount importance for all aircraft maneuvers that are performed at very low altitudes, in particular in phases such as takeoff and landing.

The analysis of the aircraft stability and control during takeoff and landing requires an accurate knowledge of the aerodynamic coefficients in ground effect.[1] Staufenbiel and Schlichting[1] analyzed the longitudinal stability of an aircraft in ground effect. It was observed that variations of the longitudinal stability caused by the ground proximity were responsible for substantial changes in the landing trajectories, especially during the flare-out maneuvers.

More recently the increased development of unmanned aerial vehicles (UAV) has resulted in the consideration of these vehicles for missions at low altitudes.[2] Many UAVs implement flight control programs to accomplish the required mission profiles and are equipped with plant control systems whose characteristics take into account the forces and moments that are developed in ground effect.[1,2]

The vehicles that are considered in this study are the "wing-in-ground-effect" (WIG) crafts, also called Ekranoplans, which are high-speed low-altitude flying vehicles that purposely utilize the favorable ground effect. WIG craft are of interest because of the peculiarities that they exhibit in comparison to conventional airplanes. Within the framework of high-speed low-altitude transportation, the high aerodynamic efficiency that these vehicles achieve together with low wing aspect ratios and low structure weights make them more suitable than conventional aircraft.[3]

During horizontal flight with $\varphi = \beta = 0$, the ground plane imposes a boundary condition on the aerodynamic field that symmetrically reduces the downward flow about the aircraft. This results in a downwash reduction at the tail together with an increase in the lift slope of both wing and tail[4] that depends on the height above the ground. However if the vehicle flies with an arbitrary orientation with respect to the inertial frame, the ground alters the vehicle aerodynamics in such a way that the pressure distribution on the aircraft depends on both height and attitude. Therefore the aerodynamic coefficients, which are a function of both height and aerodynamic angles, also vary with the Euler angles. This effect, which modifies performance and flying qualities, is observed by pilots when an aircraft is flown close to the ground. For example, during flight tests on WIG vehicles[5] horizontal banked turns were carried out to demonstrate that the sideslip, rudder, and ailerons angles are quite different from those needed out of ground effect. Although these angles are quite small for steady banked turns out of ground effect, for a WIG craft they are quite large. Kornev and Matveev[5] considered the effect of the roll angle and proposed semi-empirical expressions for the aerodynamic coefficients, which are based on results from numerical simulations. They noted that, during a banked turn near the ground, the vehicle develops additional aerodynamic forces and moments that depend upon the roll angle.

From a safety perspective, a banked turn must be performed with a limited roll angle and at a high enough altitude to avoid the risk of touchdown. Thus, a special maneuver strategy is adopted to maintain the distance between the wing tip and ground surface.[5] This maneuver requires a very large turning radius that strongly reduces the maneuverability of the aircraft. For this reason it is prudent to use a control system to minimize the turning radius.[6] The design of such controllers requires a knowledge of the aerodynamic coefficients that are developed in ground effect,[6] while also accounting for the influence of the attitude on aircraft's forces and moments.

Another source of the significant variations of the aerodynamic coefficients of a WIG craft is nonzero sink rates. The vertical velocity of the aircraft determines the unsteady or dynamic ground effect, which, in turn, produces aerodynamic forces and moments that depend upon the flight-path angle. Such an effect occurs during WIG maneuvers as in the case of the vertical jumping,[5] which is very short climbing phase that is used to avoid collisions with low obstacles.

In the present work the flight dynamics of an aircraft in ground effect are examined through an analytical procedure that estimates the aerodynamic forces and moments and takes into account the aforementioned effects, such as attitude and sink rate.

In previous work Chang and Muirhead[7] experimentally examined the forces on low-aspect-ratio wings with sink rate. Nuhait and Mook[8] numerically examined the phenomena using an unsteady vortex-lattice method. Nuhait and Zedan[9] analyzed the unsteadiness induced by the vertical velocity using a vortex lattice method, with a predetermined wake shape. More recently Han et al.[10] investigated the two-dimensional ground effect of flat plates in tandem configuration using a discrete vortex method. They observed that the unsteadiness has a marked impact on the performance of a tandem configuration.

In Ref. 11, a mathematical model of flow about lifting bodies, in steady and unsteady ground effect, is presented. The linearized equations of motion for the longitudinal dynamics, in which the aerodynamic coefficients are expressed by means of linear derivatives with respect height, pitch angle, and their time derivatives, are developed. Kumar[12] examined the dynamics of a WIG craft including the effect of a perturbation in the forward velocity; the stability of the WIG craft was also examined from an eigenvalue analysis of the linearized equations of motion. Staufenbiel[13] analyzed the longitudinal stability of aircraft in ground effect using the characteristic equation. The nonlinear effects were also examined by numerical calculation of the time histories of the motion equations.

Although other references to the aerodynamic forces and moments in the ground effect[14–16] can be found, to the author's knowledge the effects exerted by the attitude of the aircraft on the flight dynamics have not been examined. Therefore the objective of the present work is to develop an accurate mathematical model that can be used for the analysis of the performance and flying qualities of aircraft in ground effect.

In the present work the aerodynamic forces and moments are derived from the Lagrange equations. The Lagrangian function of the physical problem is given by the kinetic energy of the airstream, which is expressed in terms of the aerodynamic and Euler angles. This approach allows the forces and moments in ground effect to be accurately formulated and the variations in the performance and flying quality to be interpreted.

Equations of Motion

In this section the rigid aircraft equations of motion, which are used to study the vehicle dynamics in ground effect, are presented. These equations are written in the form[4]

$$m(\dot{\boldsymbol{v}} + \boldsymbol{\omega} \times \boldsymbol{v}) = \boldsymbol{F}^e, \qquad \boldsymbol{J}\dot{\boldsymbol{\omega}} + \boldsymbol{\omega} \times \boldsymbol{J}\boldsymbol{\omega} = \boldsymbol{Q}^e \tag{1}$$

$$\dot{\boldsymbol{r}} = \boldsymbol{L}^T \boldsymbol{v}, \qquad \dot{\boldsymbol{\Phi}} = \boldsymbol{R}^{-1} \boldsymbol{\omega} \tag{2}$$

The elements of the diagonal matrix $\boldsymbol{J}$ are

$$J_{xx} = 0.02mb^2, \qquad J_{yy} = 0.02ml^2, \qquad J_{zz} = 0.02m(b^2 + l^2)$$

$\boldsymbol{F}^e = \boldsymbol{T} + m\boldsymbol{Lg} + \boldsymbol{F} + \boldsymbol{F}_v$ and $\boldsymbol{Q}^e = \boldsymbol{Q}$ are the sum force and the moment with respect to center of gravity of the external forces, where $m\boldsymbol{Lg}$ represents the weight force expressed in body axes. $\boldsymbol{F}_v$, which has a purely dissipative action, is the aerodynamic viscous force that is given as $\boldsymbol{F}_v = -\frac{1}{2}\rho V^2 S C_{D_f}(\cos\alpha\cos\beta, \sin\beta, \sin\alpha\cos\beta)$, with $C_{D_f} = 0.047$ that does not depend on ground effect. Thus $\boldsymbol{F} + \boldsymbol{F}_v$ and $\boldsymbol{Q}$ are, aerodynamic force and moment, which, in body axes, are expressed as

$$\boldsymbol{F} + \boldsymbol{F}_v \equiv \begin{bmatrix} X \\ Y \\ Z \end{bmatrix} = \frac{1}{2}\rho V^2 S \begin{bmatrix} C_x \\ C_y \\ C_z \end{bmatrix}$$

$$\boldsymbol{Q} \equiv \begin{bmatrix} L \\ M \\ N \end{bmatrix} = \frac{1}{2}\rho V^2 S \begin{bmatrix} bC_l \\ cC_m \\ bC_n \end{bmatrix} \tag{3}$$

The aircraft is assumed to be equipped by a propulsive system, which is a constant speed propeller driven by a reciprocating engine. Thus, the thrust force $\boldsymbol{T}$, which is aligned with x_B, is calculated by dividing the propulsive power $\Pi_{\max}\delta_T\eta$ by the velocity component u, where the propeller efficiency η is assumed to be constant and equal to 0.82.

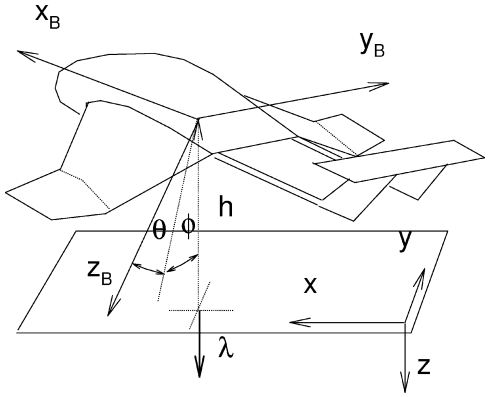

Fig. 1 Influence of φ and ϑ on a vehicle in ground effect.

Analysis

The goal of the present section is to examine how the attitude acts upon the flowfield about a vehicle flying in ground effect. Consider Fig. 1, a rigid aircraft that moves in a potential flow and in close proximity to a rigid surface of infinite extent. The attitude is represented by the vector

$$\boldsymbol{\lambda} \equiv (-\sin\vartheta, \sin\varphi\cos\vartheta, \cos\varphi\cos\vartheta) \tag{4}$$

which is the normal unit vector of the ground surface in body frame. The wakes behind the body are considered to be rigid, and their shedding lines are assigned. Therefore the velocity potential is the scalar product between the derivative of the potential with respect to the velocity and the flight velocity $\boldsymbol{v}$ in body frame,[17] that is,

$$\phi = \frac{\partial\phi}{\partial\boldsymbol{v}}\cdot\boldsymbol{v} \equiv \frac{\partial\phi}{\partial\boldsymbol{v}}\cdot(\cos\alpha\cos\beta, \sin\beta, \sin\alpha\cos\beta)V \tag{5}$$

Because the velocity potential satisfies the Laplace equation and satisfies the integral equations derived from the application of the Green's second identity, the derivative of the potential with respect to the velocity is given by the sum of surface integrals.[17]

This derivative can be written in terms of $\boldsymbol{\lambda}$ as

$$\frac{\partial\phi}{\partial\boldsymbol{v}} = \frac{\partial\phi_0}{\partial\boldsymbol{v}} + \frac{\partial^2\phi_0}{\partial\boldsymbol{v}\partial\boldsymbol{\lambda}}(\boldsymbol{\lambda}-\boldsymbol{\lambda}_0) \tag{6}$$

where $\partial^2\phi/\partial\boldsymbol{v}\partial\boldsymbol{\lambda} \equiv ((\partial^2\phi/\partial v_i\partial\lambda_j))$ is the matrix of the second-order derivatives of the potential.

Whereas Eq. (5) yields the relationship between ϕ and the aerodynamic angles, the second term of Eq. (6) accounts for the effect of the attitude on the vehicle aerodynamics. The kinetic energy of the airstream using Eqs. (5) and (6) is

$$T = \frac{1}{2}\rho\iint_{S_v}\boldsymbol{v}\cdot\boldsymbol{n}\phi\,\mathrm{d}S = \frac{1}{2}\boldsymbol{v}\cdot\boldsymbol{M}\boldsymbol{v} + \frac{1}{2}\boldsymbol{v}\cdot\{\boldsymbol{H}(\boldsymbol{\lambda}-\boldsymbol{\lambda}_0)\}\boldsymbol{v} \tag{7}$$

where

$$\boldsymbol{M} = \iint_{S_v}\frac{\partial\phi_0}{\partial\boldsymbol{v}}\otimes\boldsymbol{n}\,\mathrm{d}S, \qquad \boldsymbol{H} = \iint_{S_v}\frac{\partial^2\phi_0}{\partial\boldsymbol{v}\partial\boldsymbol{\lambda}}\otimes\boldsymbol{n}\,\mathrm{d}S \tag{8}$$

are second- and the third-order tensors. Equation (7) describes the kinetic energy of the stream in terms of aerodynamic angles; the effect of the vehicle attitude is accounted for through the second term, where the quantity $\boldsymbol{H}(\boldsymbol{\lambda}-\boldsymbol{\lambda}_0)$ is a second-order tensor that is calculated as $\boldsymbol{H}(\boldsymbol{\lambda}-\boldsymbol{\lambda}_0) \equiv H_{ijk}(\lambda_k - \lambda_{k0})$.

It is worthwithe to highlight some characteristics of the kinetic energy. First, for flat ground the heading angle does not modify the aerodynamic field about the aircraft; therefore, in Eq. (7) the kinetic energy does not depend on ψ. Furthermore, because of the vehicle symmetry about the plane (x_B, z_B) T is an even function of φ and β. Therefore both $\boldsymbol{M}$ and $\boldsymbol{H}$ are expressed in the form

$$\boldsymbol{M} = \begin{bmatrix} M_{11} & 0 & M_{13} \\ 0 & M_{22} & 0 \\ M_{13} & 0 & M_{33} \end{bmatrix}, \qquad \boldsymbol{H} = \begin{bmatrix} \boldsymbol{h}_{11} & 0 & \boldsymbol{h}_{13} \\ 0 & \boldsymbol{h}_{22} & 0 \\ \boldsymbol{h}_{13} & 0 & \boldsymbol{h}_{33} \end{bmatrix} \tag{9}$$

with $\boldsymbol{h}_{ij} \equiv (h_{ij1}, 0, h_{ij3})$, $i, j \neq 2$.

Equations (8) establish that $\boldsymbol{M}$ and $\boldsymbol{H}$ are functions of h/c that do not vary with the Euler and aerodynamic angles. In the present work, both the tensors $\boldsymbol{M}$ and $\boldsymbol{H}$ are expressed in terms of the dimensionless height through the parameter τ (Ref. 11)

$$f = f_\infty + f_1\tau + f_2\tau^2 \tag{10}$$

Calculation Method

In the equations of motion, the representation of the aerodynamic force and moment coefficients in terms of the Euler angles, flight-path angle, and dimensionless height, is necessary to interpret the performance and flying qualities in ground effect. This section deals with the calculation of aerodynamic actions developed by a vehicle in ground proximity. The procedure presented here allows the calculation of the aerodynamic forces and moments through the Lagrange equation method. This approach has been already applied to the calculation of the aerodynamic forces and moments of ultralight aircraft that are flown in the presence of a wind gradient.[18] To derive the expression of force and moment, the kinetic energy of the potential flow that is generated by the vehicle is considered. Then the aerodynamic force $\boldsymbol{F}$ and moment $\boldsymbol{Q}$ are calculated using the Lagrange equation method in the general form[17,18]:

$$\boldsymbol{F} = -\frac{\mathrm{d}}{\mathrm{d}t}\frac{\partial T}{\partial\boldsymbol{v}} - \boldsymbol{\omega}\times\frac{\partial T}{\partial\boldsymbol{v}} \tag{11}$$

$$\boldsymbol{Q} = \boldsymbol{Q}_{\mathrm{a.c.}} + (\boldsymbol{r}_{\mathrm{a.c.}} - \boldsymbol{r}_{\mathrm{c.g.}})\times\boldsymbol{F} \equiv -\boldsymbol{v}\times\frac{\partial T}{\partial\boldsymbol{v}} + (\boldsymbol{r}_{\mathrm{a.c.}} - \boldsymbol{r}_{\mathrm{c.g.}})\times\boldsymbol{F} \tag{12}$$

Substituting into Eqs. (11) and (12) the expression of T that is given by Eq. (7), the aerodynamic force and moment are

$$\boldsymbol{F} = -[\dot{\boldsymbol{M}} + \dot{\boldsymbol{H}}(\boldsymbol{\lambda}-\boldsymbol{\lambda}_0)]\boldsymbol{v} - \boldsymbol{H}\dot{\boldsymbol{\lambda}}\boldsymbol{v} - \boldsymbol{\omega}\times[\boldsymbol{M} + \boldsymbol{H}(\boldsymbol{\lambda}-\boldsymbol{\lambda}_0)]\boldsymbol{v} \tag{13}$$

$$\boldsymbol{Q} = -\boldsymbol{v}\times\boldsymbol{M}\boldsymbol{v} - \boldsymbol{v}\times[\boldsymbol{H}(\boldsymbol{\lambda}-\boldsymbol{\lambda}_0)]\boldsymbol{v} + (\boldsymbol{r}_{\mathrm{a.c.}} - \boldsymbol{r}_{\mathrm{c.g.}})\times\boldsymbol{F} \tag{14}$$

Equation (13) states that $\boldsymbol{F}$ is the sum of three terms, the first of which contains the two quantities $\dot{\boldsymbol{M}}$ and $\dot{\boldsymbol{H}}$, which are

$$\dot{\boldsymbol{M}} = \frac{\partial\boldsymbol{M}}{\partial\boldsymbol{r}_w}\boldsymbol{v} + \frac{\partial\boldsymbol{M}}{\partial h}V\sin\gamma \equiv \frac{\partial M_{ij}}{\partial r_{\mathrm{kw}}}v_k + \frac{\partial M_{ij}}{\partial h}V\sin\gamma$$

$$\dot{\boldsymbol{H}} = \frac{\partial\boldsymbol{H}}{\partial\boldsymbol{r}_w}\boldsymbol{v} + \frac{\partial\boldsymbol{H}}{\partial h}V\sin\gamma \equiv \frac{\partial H_{ijk}}{\partial r_{\mathrm{lw}}}v_l + \frac{\partial H_{ijk}}{\partial h}V\sin\gamma \tag{15}$$

According to the classical lifting bodies theory, $\dot{\boldsymbol{M}}$ and $\dot{\boldsymbol{H}}$ are proportional to the velocity circulation around the aircraft. They represent the time derivatives of $\boldsymbol{M}$ and $\boldsymbol{H}$, which are related to the shedding wake surfaces past the aircraft and to the sink rate. $\partial\boldsymbol{M}/\partial\boldsymbol{r}_w$ and $\partial\boldsymbol{H}/\partial\boldsymbol{r}_w$ are the apparent mass terms relative to the unit of wake length $\boldsymbol{r}_w$, which gives the aerodynamic force developed in horizontal flight, whereas both $\partial\boldsymbol{M}/\partial h$ and $\partial\boldsymbol{H}/\partial h$ produce the unsteady ground effect when $\gamma \neq 0$. This last result is a consequence of the observation that the pressure on the vehicle surface depends on the sink rate through the Bernoulli theorem $p = \rho(\mathrm{const} - (\boldsymbol{v}\cdot\boldsymbol{v})/2 - \partial\phi/\partial t)$, where $\boldsymbol{v}$ is the local velocity of the stream and $\partial\phi/\partial t = (\partial\phi/\partial h)(V\sin\gamma)$ is the unsteady term caused by the sink rate. The second term in Eq. (13) depends on $\dot{\boldsymbol{\lambda}}$ and represents a force that varies with the angular velocity. In fact it can be written taking into account that $\dot{\boldsymbol{\lambda}}$ is related to the angular velocity through Eq. (2)

$$\dot{\boldsymbol{\lambda}} = \frac{\partial\boldsymbol{\lambda}}{\partial\boldsymbol{\Phi}}\dot{\boldsymbol{\Phi}} = \frac{\partial\boldsymbol{\lambda}}{\partial\boldsymbol{\Phi}}\boldsymbol{R}^{-1}\boldsymbol{\omega} \tag{16}$$

where

$$\frac{\partial\boldsymbol{\lambda}}{\partial\boldsymbol{\Phi}} = \begin{bmatrix} \frac{\partial\lambda_x}{\partial\varphi} & \frac{\partial\lambda_x}{\partial\vartheta} & \frac{\partial\lambda_x}{\partial\psi} \\ \frac{\partial\lambda_y}{\partial\varphi} & \frac{\partial\lambda_y}{\partial\vartheta} & \frac{\partial\lambda_y}{\partial\psi} \\ \frac{\partial\lambda_z}{\partial\varphi} & \frac{\partial\lambda_z}{\partial\vartheta} & \frac{\partial\lambda_z}{\partial\psi} \end{bmatrix} \equiv \begin{bmatrix} 0 & -\cos\vartheta & 0 \\ \cos\varphi\cos\vartheta & -\sin\varphi\sin\vartheta & 0 \\ -\sin\varphi\cos\vartheta & -\cos\varphi\sin\vartheta & 0 \end{bmatrix} \tag{17}$$

Hence, this is a contribution to the rotational derivatives that tend to zero as $h/c \to \infty$. Also the last term of Eq. (13) gives a contribution to the rotational derivatives, which in turn depends upon the height and vehicle attitude.

In Eq. (14) for the moment, the first term is a function of α and β, whereas the second term is a function of the attitude variations.

Thus, force and moment are

$$\boldsymbol{F} = -\left\{\frac{\partial \boldsymbol{M}}{\partial h} V \sin\gamma + \frac{\partial \boldsymbol{M}}{\partial \boldsymbol{r}_w}\boldsymbol{v} + \left[\frac{\partial \boldsymbol{H}}{\partial h} V \sin\gamma + \frac{\partial \boldsymbol{H}}{\partial \boldsymbol{r}_w}\boldsymbol{v}\right](\boldsymbol{\lambda} - \boldsymbol{\lambda}_0)\right\}\boldsymbol{v}$$

$$-\left\{\boldsymbol{H}\frac{\partial \boldsymbol{\lambda}}{\partial \boldsymbol{\Phi}}\boldsymbol{R}^{-1}\boldsymbol{\omega}\right\}\boldsymbol{v} - \boldsymbol{\omega} \times \{\boldsymbol{M} + \boldsymbol{H}(\boldsymbol{\lambda} - \boldsymbol{\lambda}_0)\}\boldsymbol{v} \tag{18}$$

$$\boldsymbol{Q} = -\boldsymbol{v} \times \{\boldsymbol{M} + \boldsymbol{H}(\boldsymbol{\lambda} - \boldsymbol{\lambda}_0)\}\boldsymbol{v} + (\boldsymbol{r}_{\text{a.c.}} - \boldsymbol{r}_{\text{c.g.}}) \times \boldsymbol{F} \tag{19}$$

Therefore, Eqs. (18) and (19) allow the determination of $\boldsymbol{F}$ and $\boldsymbol{Q}$ in ground proximity and account for the attitude and sink rate.

Validation of the Method

To validate the method, several comparisons with existing data in the literature are presented.

The aerodynamic force and moment coefficients are evaluated from Eqs. (13) and (14), where $\boldsymbol{M}$ and $\boldsymbol{H}$ are numerically calculated using Eq. (8). The velocity potential is computed by an unsteady vortex-lattice code, developed by the author, that takes into account the ground effect using the method of images. Specifically the presence of the ground is simulated by placing a specular image of the lifting body at an equal distance below the ground plane. Thus, two symmetrically positioned lifting bodies are considered to determine a flat ground surface.

The results of the first case are presented in Fig. 2a. The figure shows increments of the lift coefficient in terms of h/c for a delta wing having an aspect ratio equal to 1.456; h is measured at the midpoint of the root chord. The simulation is computed for an angle of attack of 22.1 deg and a flight-path angle equal to -10 deg. The dashed line represents the data of Ref. 8, while the symbols are the experimental data of Chang and Muirhead.[7] The figure shows that the lift coefficients obtained by the present method, shown by the solid line, are in good agreement with the those of both Refs. 7 and 8.

Figures 2b–2d show, respectively, the variations of lift, drag, and pitching-moment coefficients for a delta wing having an aspect ratio of 1.456, in terms of the dimensionless height, measured at the trailing edge. The simulations are made for $\alpha = 10$ deg and $\gamma = 0, -20$ deg. The difference between the values calculated by the present method and those reported in Ref. 8 is always less than 6%.

The next case, shown in Figs. 2e–2g, shows the effect of aspect ratio on the aerodynamic coefficients. The plots show three different calculations for AR = 1.456, 1.072, and 0.705. According to Ref. 8, the height is measured at the trailing edge, and the solid symbols represent the data given in Ref. 8. The calculations show the unsteady ground effect, which is obtained for $\alpha = 10$ deg and $\gamma = -20$ deg. The results are in good agreement with those of Ref. 8.

These comparisons demonstrate that the present method provides an accurate estimation of the aerodynamic coefficients for the examined wings in steady and unsteady ground effect over a wide range of h/c variations.

Reference Vehicle

Consider a model of a vehicle sketched in Fig. 3, the main parameters of which are reported in Table 1. The vehicle is chosen according to the Lippisch Design,[19] which combines a high positioned tail with an inverted delta wing having negative dihedral along the leading edge. Such a configuration is longitudinally stable at different h/c, as a result of an adequate aerodynamic moment developed by the tail, which is located out of ground effect.[19]

The aerodynamic coefficients of the aircraft are estimated using Eqs. (18) and (19), where the matrices $\boldsymbol{M}$ and $\boldsymbol{H}$ are numerically evaluated by means of Eqs. (8).

Table 1 Dimensions and mass

Parameter	Value
Overall length l, m	6
Wing span b, m	6.8
Planform area S, m^2	16
Maximum power $\Pi_{\max}$, kW	200
Overall weight W, N	9806

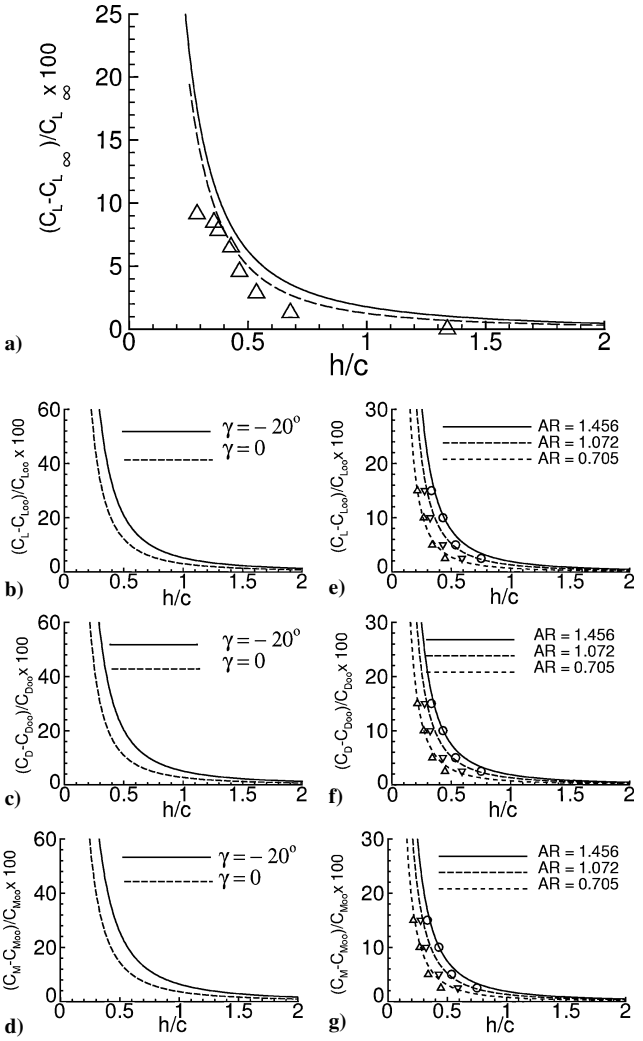

Fig. 2 Comparison of the results: a) delta wing in dynamic ground effect, where AR = 1.456, α = 22.1 deg, $\gamma = -10$, and symbols are from Ref. 7; b), c), d) delta wing in ground effect at different γ; where AR = 1.456, and $\alpha = 10$ deg; e), f), g) delta wings with different aspect ratios at $\alpha = 10$ deg, $\gamma = -20$ deg, and symbols are from Ref. 8.

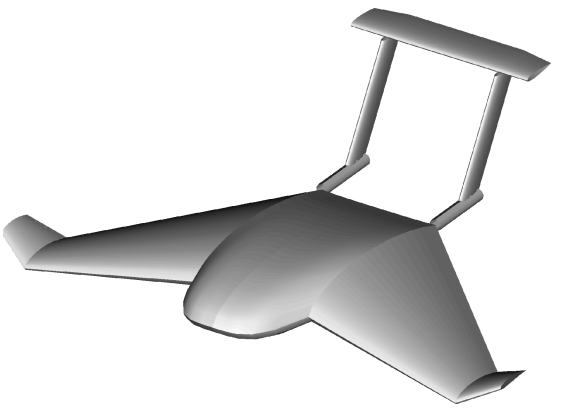

Fig. 3 Reference vehicle.

The velocity potential is calculated by the boundary element code VSAERO,[20] which is capable of solving the complex aerodynamic field around an aircraft in the presence of the ground.

The incremental aerodynamic coefficients caused by the control angles are assumed to be constant in any situation. They are

$$\Delta C_x = -0.029\delta_e^2 - 0.0493\delta_r^2 - 0.113\delta_a^2$$

$$\Delta C_y = 0.157\delta_r$$

$$\Delta C_z = -0.32\delta_e - 0.0112\delta_r^2 + 0.1352\delta_a^2$$

$$\Delta C_l = -0.07\delta_a + 0.04\delta_r$$

$$\Delta C_m = -0.923\delta_e + 0.20\delta_a^2 - 0.0055\delta_r^2$$

$$\Delta C_n = +0.0035\delta_a - 0.072\delta_r \qquad (20)$$

where the control angles are expressed in radian.

The results that deal with the vehicle characteristics in ground effect are next presented. In the subsequent figures the lines represent the calculation made using Eqs. (18) and (19), whereas the symbols indicate the aerodynamic coefficients derived from surface integrals of the pressure forces computed in the code.

Figure 4 shows how the aerodynamic characteristics vary with the height. The lift coefficient and aerodynamic efficiency in steady ground effect are shown in terms of the angle of attack for $h/c = 0.167, 0.614, 2.792, \infty$, with $\varphi = \beta = 0$. The variations in C_L are similar to the corresponding data presented in Ref. 1, whereas C_L/C_D, whose maximum value varies from about 7 (out-of-ground effect) to more than $12(h/c = 0.167)$, is in good qualitative agreement with the data presented in Ref. 11.

The influence of the pitch angle on the aerodynamic coefficients in steady ground effect is shown in Fig. 5 for C_L, C_D, and C_m vs ϑ. The calculations are carried out at $h/c = 1$, with $\gamma = \beta = \varphi = 0$, for the two cases $\boldsymbol{H} = 0$ (dashed lines) and $\boldsymbol{H} \neq 0$ (solid lines). The case with $\boldsymbol{H} = 0$ corresponds to the usual assumption of the aerodynamic coefficients that do not depend on φ and ϑ, whereas the calculation with $\boldsymbol{H} \neq 0$ accounts for the attitude effects. It is worthwhile to emphasize that the pitch angle produces marked variations on all of the aerodynamic coefficients. In the case $\boldsymbol{H} \neq 0$, C_L and C_D exhibit significant increments when $\vartheta > 0$, while the attitude acts upon the pitching moment so as to result in a quasilinear variation of $C_m(\vartheta)$. For each coefficient, the maximum percentage differences between the two cases can reach 20% of the corresponding value calculated at $\varphi = \vartheta = 0$.

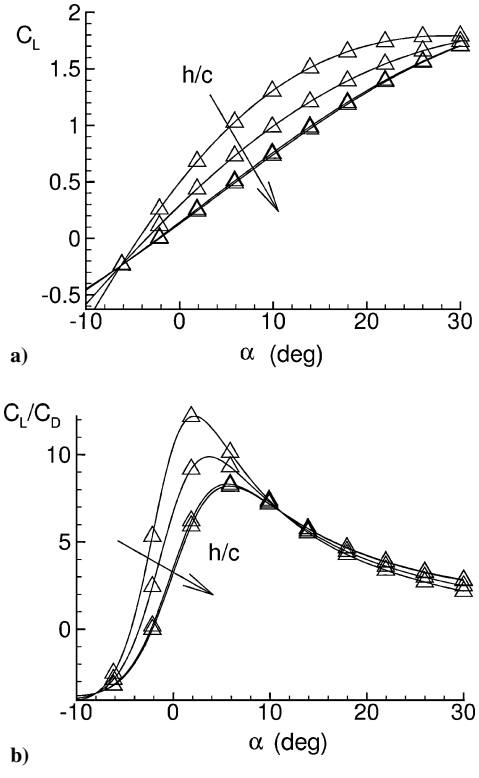

Fig. 4 Vehicle lift coefficient and aerodynamic efficiency in ground effect obtained for $h/c = 0.167, 0.614, 2.792, \infty$, at $\varphi = \beta = 0$.

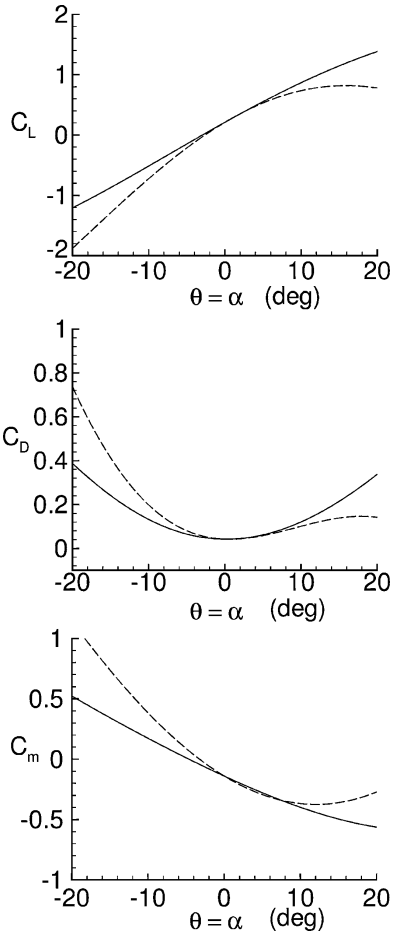

Fig. 5 Influence of pitch angle on the aerodynamic coefficients: $h/c = 1$, and $\gamma = \beta = \varphi = 0$.

The effects of the lateral attitude are next examined. Figure 6 shows all of the aerodynamic coefficients in body axis in terms of roll angle, calculated for $\alpha = 5$ deg and $\beta = \gamma = 0$. Because of the vehicle symmetry, the longitudinal coefficients C_x, C_z, and C_m, and the lateral ones C_y, C_l, and C_n are, respectively, even and odd functions of φ. For $|\varphi| < 10$ deg, the increment in the longitudinal coefficients can be greater than 15% for $h/c < 1$. Note that the variations of C_x and C_z correspond to increases of C_L/C_D that can lead to an improvement in the vehicle performance during turning maneuvers. As far as the lateral coefficients are concerned, linear variations are observed, for $h/c < 1$ that can be greater than those caused by a sideslip angle $|\beta| = |\varphi|$. Therefore, the attitude effects modify the force and moment coefficients; the degree of change depends upon the dimensionless height.

The influence of the flight-path angle on the aerodynamic coefficients is next examined. Figure 7 shows C_L, C_D, and C_m in terms of h/c, for $\gamma = -5$ deg, 0, + 5 deg. In these results, for which $\alpha = 5$ deg, $\beta = \varphi = 0$, it is evident that the ground effect is stronger for negative flight-path angles at relatively low h/c.

The proposed model also includes the effects of angular velocity. Force and moment rotational derivatives are calculated from the derivative of Eqs. (18) and (19) with respect to p, q, and r. Figure 8 shows the dimensionless longitudinal rotational derivative in terms of the angle of attack, calculated at $\beta = \varphi = 0$, for various h/c. Large variations in the derivative can be seen.

Comparisons between the present results and those reported in Kornev and matveev[5] and Staufenbiel[13] are next presented. In Ref. 5,

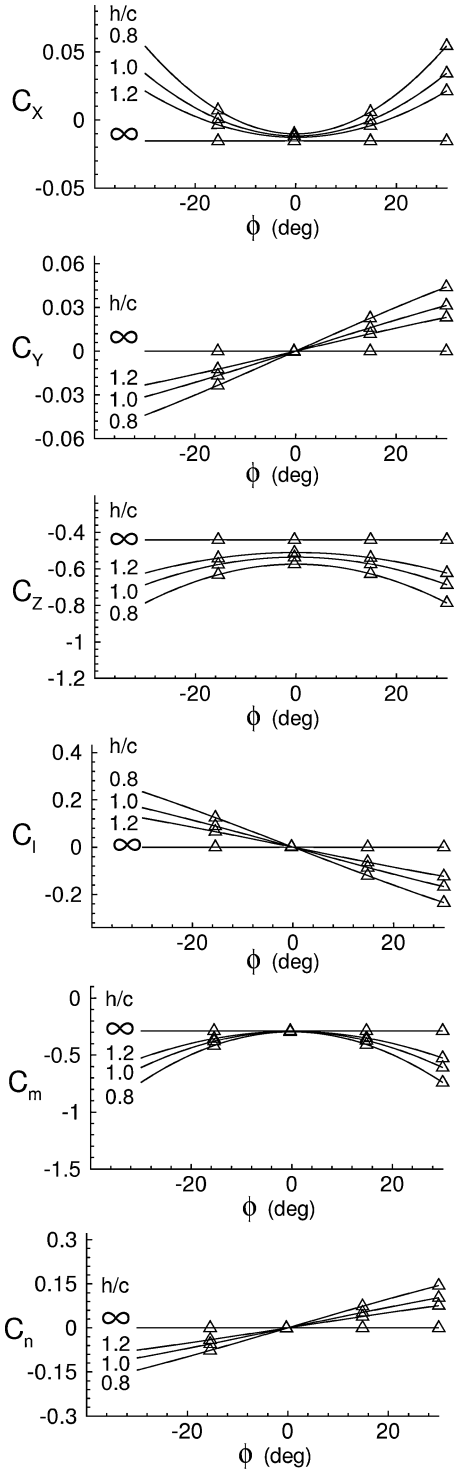

Fig. 6 Influence of roll angle on the aerodynamic coefficients: $\alpha = 5$ deg, and $\beta = \gamma = 0$.

the rotational derivative C_{Lq} of the WIG craft ELA01 is given. Figure 9 shows the comparison between the derivatives obtained in Ref. 5 (horizontal axis) and these calculated using the proposed method (vertical axis). In Fig. 9a the derivative C_{Lq} calculated at $h/c = 0.1$ is represented, whereas Fig. 9b reports $C_{L\gamma}$ and $C_{m\gamma}$. Although the vehicle is geometrically different with respect to the reference vehicle, the present results are in relatively good agreement with the data of Ref. 5. As for Ref. 13, the data concern the WIG craft X-113, which is also designed according to the Lippish criteria. Although the two vehicles have some geometrical differences, Table 2 shows that the aerodynamic coefficients calculated by the present method are in good agreement with those from Ref. 13.

Table 2 Dimensionless aerodynamic derivatives vs h/c[a]

h/c	∞		1.0		0.4	
C_{L_α}	(3.0)	3.47	(3.2)	3.7	(3.6)	4.02
C_{L_h}	(0.0)	0.0	(−0.035)	−0.042	(−0.35)	−0.38
C_{m_α}	(−0.68)	−0.7	(−0.70)	−0.73	(−0.73)	−0.76
C_{m_h}	(0.0)	0.0	(0.003)	0.0037	(0.055)	0.063
C_{m_q}	(−4.44)	−4.20	(−4.44)	−4.03	(−4.44)	−3.97

[a]The values in the parenthesis are from Ref. 13.

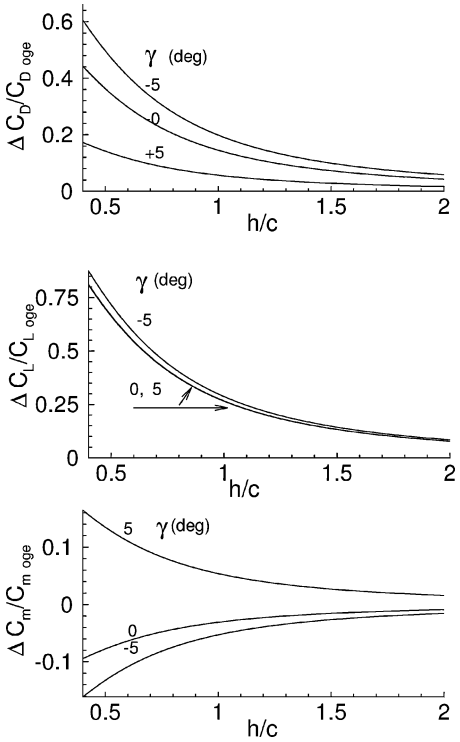

Fig. 7 Influence of flight-path angle on the aerodynamic coefficients: $\alpha = 5$ deg, and $\beta = \varphi = 0$.

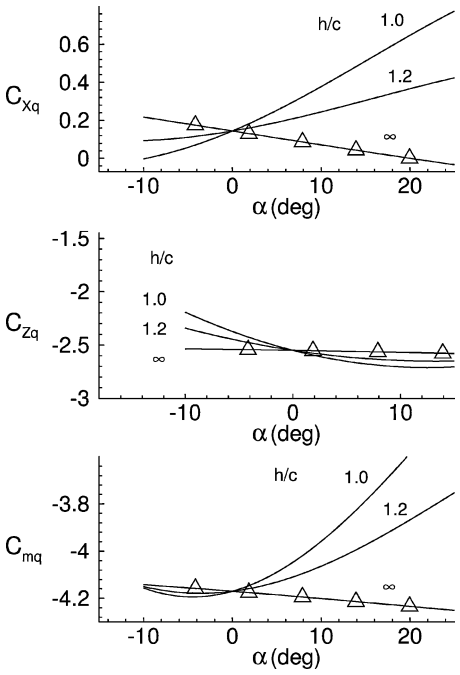

Fig. 8 Vehicle rotational derivatives in ground effect in function of the angle of attack: $\beta = \varphi = 0$.

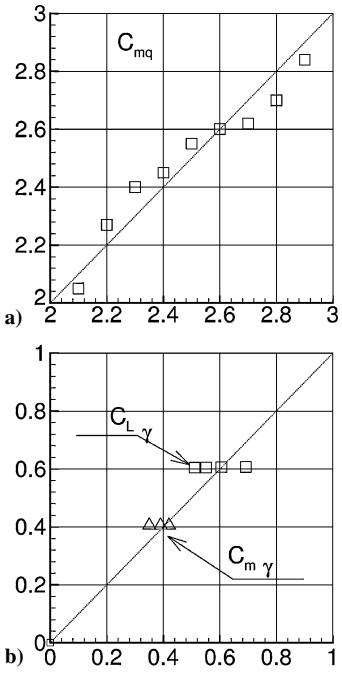

Fig. 9 Comparison of the dimensionless aerodynamic derivatives for $h/c = 0.1$. Data from Ref. 5 in horizontal axis, present results in vertical axis.

Results and Discussions

In what follows, to study the influence of the ground effect on state and control variables at trim some significant situations that correspond to the level and turning flight will be considered. Furthermore the vehicle stability will be investigated by means of the eigenvalues analysis applied to the linearized motion equations, whereas the nonlinear analysis of the vehicle motion will be made integrating the full set of the equations of motion.

Equations (1) and (2) are used as equations of motion, and the contribution of the three control angles to the aerodynamic forces and moments is taken into account through incremental force and moment coefficients as reported in Eqs. (20).

As a first result, Fig. 10 summarizes the trim condition in level flight for $\beta = 0$ at different h/c. The diagrams show the angle of attack, elevator angle, and required throttle in terms of the flight speed.

Because in ground effect the lift coefficient increases when h/c diminishes, the angle of attack decreases with h/c (Fig. 10a). The δ_e (Fig. 10b) monotonically increases with V, which indicates that there is a stable behavior except the lower velocities and altitudes, where the curves show decreasing branches ($h/c < 1$). This last feature only occurs at high angle of attack and is the result of the simultaneous effects of ϑ and α on the aerodynamic forces and pitching moment. Figure 10c shows the required throttle as a function of the flight speed. Each curve exhibits a distinct minimum value that increases with h/c. Because the ground effect is stronger at high angle of attack, the throttle for $h/c = 0.5$, and 1 is less than the throttle for $h/c \to \infty$ only for $V < 55$ ms^{-1}.

To evaluate the attitude effect on symmetric flight situations, two different trim conditions in straight flight, at $h/c = 1$, are examined (Fig. 11). The continuous and dashed lines indicate the solutions calculated for $\boldsymbol{H} \neq 0$ and $\boldsymbol{H} = 0$, respectively. The two solutions show substantial divergences, which are caused by the different aerodynamic coefficients in the two cases. At lower flight speeds the angle of attack shows important differences between the two solutions (Fig. 11a), whereas minor divergences are evident in Fig. 11b, where the elevator angle is displayed. The little angles of attack obtained for $\boldsymbol{H} \neq 0$ are in agreement with the data given in Fig. 5, which shows relatively high lift coefficients when the attitude effects are accounted for. As a result, for $\boldsymbol{H} \neq 0$ lower flight speeds than those calculated for $\boldsymbol{H} = 0$ are obtained. Also the required throttle (Fig. 11c) depends upon the attitude. In fact, ϑ acts on the aerodynamic forces in such

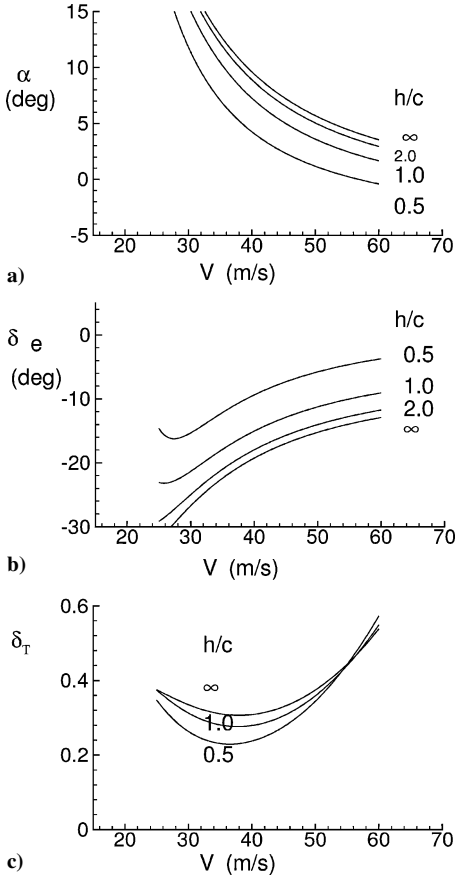

Fig. 10 Trim calculation in horizontal flight at different heights: $\beta = \varphi = 0$.

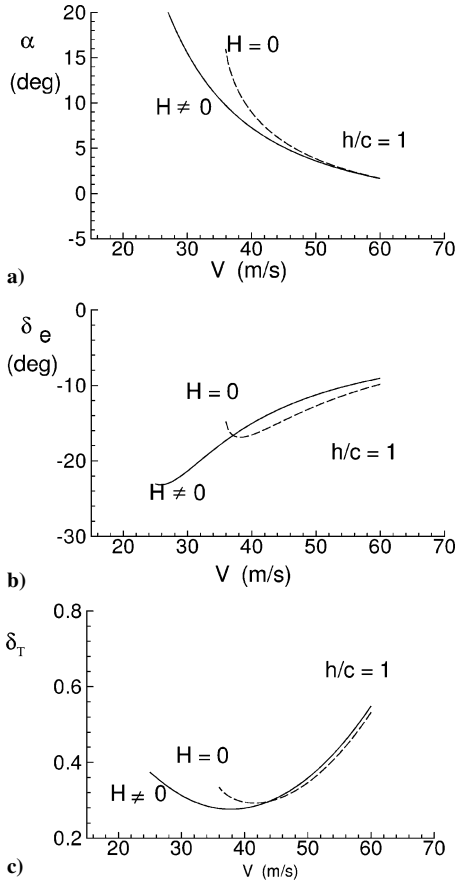

Fig. 11 Influence of the attitude on the trim in horizontal flight.

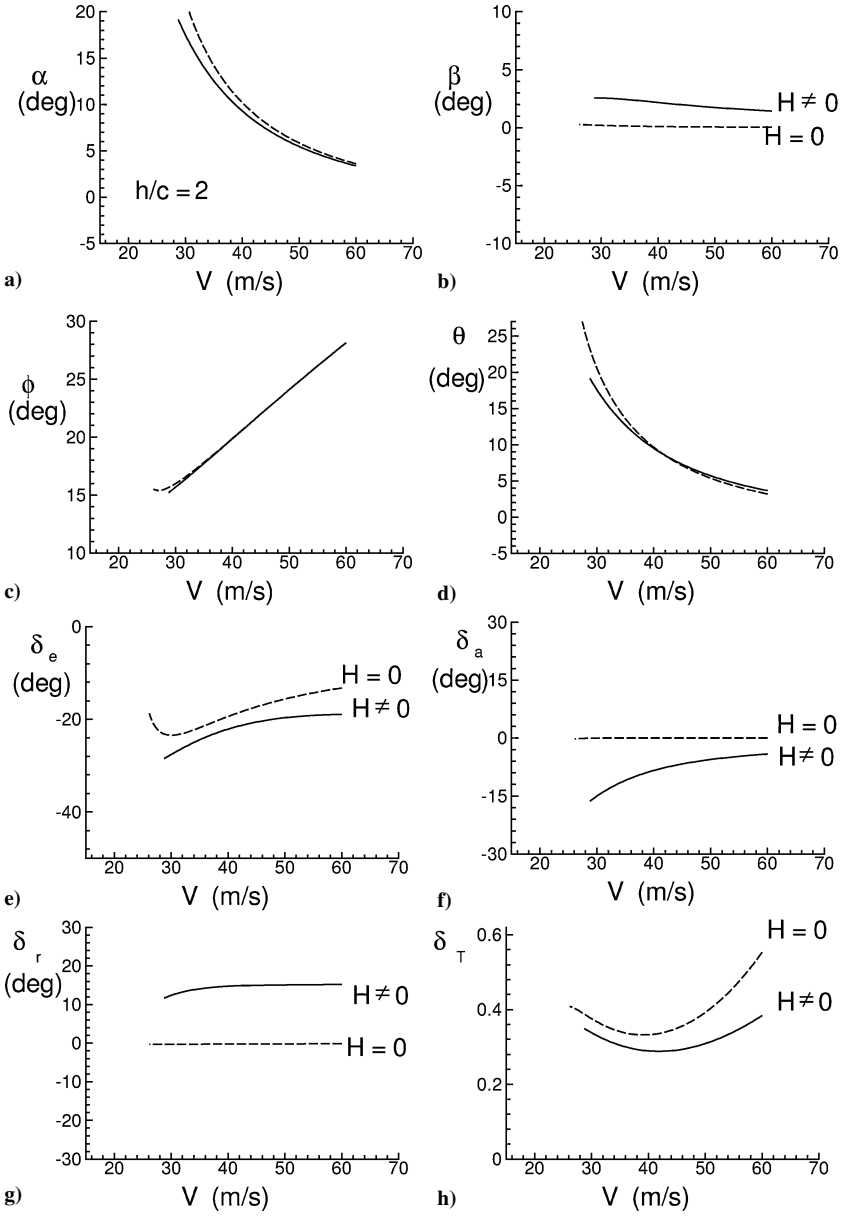

Fig. 12 Trim analysis of a truly banked turn with $\zeta = 5$ deg/s^{-1}.

a way that the throttle exhibits significant reductions for velocities less than 40 ms^{-1}.

The third case, shown in Fig. 12, analyzes the effect of the roll angle on a banked maneuver. The aircraft carries out a "truly banked" turn in the horizontal plane, and the angular velocity $(p, q, r) \equiv (-\sin\vartheta, \cos\vartheta \sin\varphi, \cos\vartheta \cos\varphi)\zeta$ is vertical with $\zeta = 5$ deg/s^{-1}. In this maneuver the sum of weight and centrifugal force at the aircraft c.g. is in the vehicle symmetry plane (x_B, z_B). To avoid possible touchdown during the maneuver, it is assumed that $h/c = 2$ in all situations. In the diagrams the solutions that correspond to $\boldsymbol{H} = 0$ and $\boldsymbol{H} \neq 0$ are shown. Figure 12a shows that there are higher differences in the angles of attack between the two cases at lower flight velocities. As in the case of a truly banked maneuver that is performed out of ground effect, the solution for $\boldsymbol{H} = 0$ shows very small sideslip angles (Fig. 12b), whereas for $\boldsymbol{H} \neq 0$ nonzero sideslip are observed. The reason of such discrepancy is because of φ that causes additional force and moment terms that are thus balanced by nonzero sideslip angles. The roll angle (Fig. 12c) exhibits little differences between the two solutions over the entire range of the flight speed, whereas more significant differences are seen in the pitch angle (Fig. 12d). If $\boldsymbol{H} = 0$, ailerons and rudder are very little as in a banked turn at high altitude, whereas for $\boldsymbol{H} \neq 0$ the attitude effects lead to a disagreement between the two solutions. Figure 12h shows the effect on throttle for both the cases. As a result of the aerodynamic efficiency increments caused by the nonzero roll angles (see Fig. 6), lower throttle levels are needed for $\boldsymbol{H} \neq 0$. This means that, at least in these flight conditions, the drag increment caused by the maneuver is in part counterbalanced by the drag reduction caused by φ.

The vehicle stability is next evaluated through the eigenvalue analysis applied to the linearized equations of motion, where the various modes are identified by means of the eigenvector analysis. The root locus is calculated for straight flight at the speed of 40 m/s, varying h/c from ∞ to about 1.

The attitude effects on the vehicle stability are summarized in the two sets of Figs. 13a, 13b and 13c, 13d, which show, respectively, the two cases $\boldsymbol{H} = 0$ and $\boldsymbol{H} \neq 0$. Because of the different aerodynamic force and moment coefficients developed in the two situations, the eigenvalues vary with h/c in a different manner. However, out of ground effect the vehicle shows three oscillating stable modes (which are phugoid, short period, and Dutch roll) and two aperiodic modes [which are the roll convergence (stable) and the spiral mode (unstable)].

The case $\boldsymbol{H} = 0$ is discussed first. Phugoid is a stable mode in the entire range of h/c, whose eigenvalues significantly vary for $h/c < 4$ (see Figs. 13a and 13b). Its imaginary and real parts, respectively,

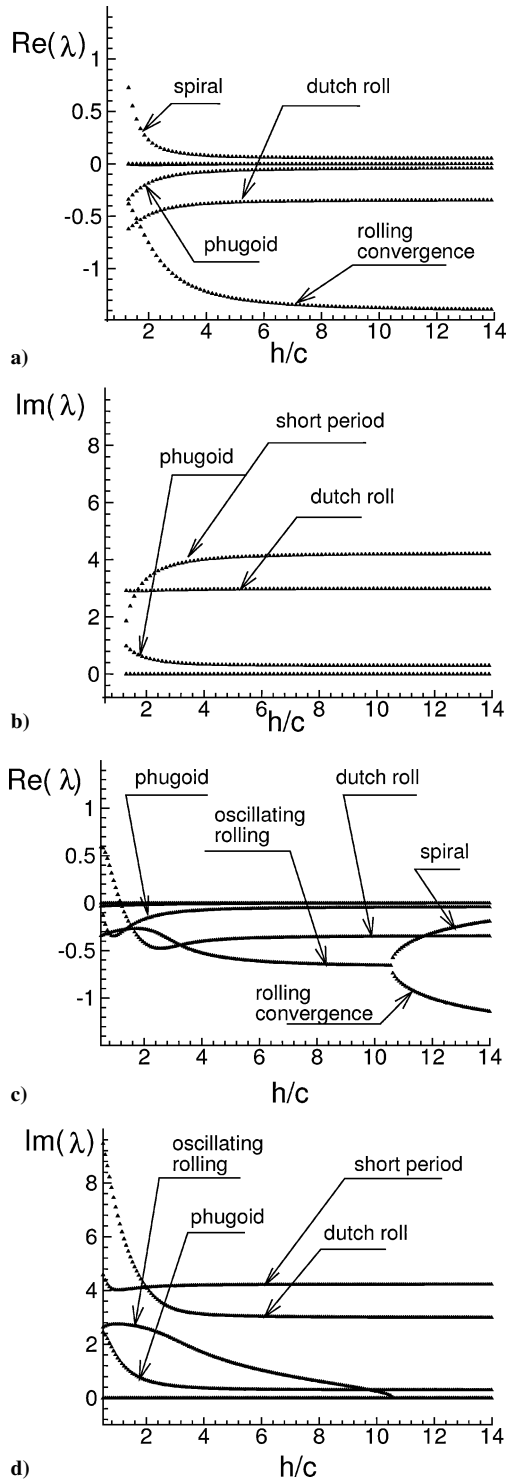

Fig. 13 Root locus: a) and b) $\boldsymbol{H}=0$, and c) and d) $\boldsymbol{H}\neq 0$.

increase and diminish as $h/c \to 0$. At each h/c the short period is a stable mode that has significant variations in the eigenvalues for $h/c < 4$ that are caused by the nonlinearities of $C_m(\vartheta)$ (see Fig. 5). The Dutch roll eigenvalues show smaller variations. Their imaginary part does not change with h/c, whereas the real part displays more marked variations. As for the nonoscillating modes, the positive eigenvalue associated with the spiral mode increases as $h/c \to 0$. Although the rolling convergence remains a stable mode, it presents a negative eigenvalue that rises as soon as h/c diminishes.

Figures 12c and 12d show the root locus for $\boldsymbol{H}\neq 0$. The attitude effect produces significant differences with respect to the preceding case. The phugoid mode exhibits the same behavior with the exception of lower h/c, where it becomes unstable (see Fig. 13c). Such instability is produced by the combined effect of both pitch angle and height upon the lift coefficient, which is more pronounced at lower h/c. With respect to the case with $\boldsymbol{H}=0$, the attitude influences the pitching moment such that the derivative $C_{m\alpha}$ is almost constant with the height; therefore, the short-period eigenvalues have smaller variations with h/c.

Pronounced discrepancies between the two cases are evident in terms of the lateral modes. It is seen that the Dutch roll eigenvalues are quite different from those of the preceding case. They show increments for $h/c < 4$ that make the mode unstable at $h/c \simeq 1.5$. More important divergence is apparent for spiral mode and rolling convergence. The spiral mode is completely changed. It becomes stable at about $h/c = 20$, whereas for $h/c \simeq 10.5$ it degenerates, together with the rolling convergence, into a new mode called oscillating rolling that is the consequence of the roll-angle influence on the aerodynamics force and moment. The oscillating rolling, which occurs under a certain h/c, is a stable oscillating mode that modifies the lateral stability. Also the rolling convergence depicts nonnegligible variations. Its eigenvalue strongly varies for $11 < h/c < 20$, whereas, as seen, for $h/c \simeq 10.5$ it disappears.

In the reported calculations the attitude considerably changes the lateral stability of the vehicle. The stabilization of the spiral mode, the disappearance of both spiral and rolling convergence, and the subsequent genesis of the oscillating rolling yield a rather different lateral stability than one where the attitude is not accounted for.

To estimate the dynamic response, time histories, which are calculated by integrating the full set of the motion equations, for $\boldsymbol{H}\neq 0$ are next examined. The first simulation takes place in the vertical plane at various initial heights h_0, where the vehicle, initially in level flight at equilibrium at the speed of 40 ms^{-1}, is perturbed by a pitch rate of 0.8 s^{-1}. Figure 14 gives the time histories of the perturbed height and angle of attack. In the diagrams phugoid and short-period modes can be seen. Note that the characteristic times of both the modes are in agreement with the eigenvalues calculated earlier. In all of the cases, the phugoid mode is persistent during the entire simulation period, whereas the short period, because of its strong damping, only acts at the beginning of the motion. As seen in Fig. 13, as soon as h_0/c diminishes the phugoid period decreases, and its amplitude is more damped.

The second case, shown in Fig. 15, concerns a perturbed lateral motion, where the initial condition is the same one of the preceding case, while the perturbed action is now given by a roll rate of 0.2 s^{-1}. Out of ground effect ($h_0/c \to \infty$), it is possible to identify rolling convergence, Dutch roll, and spiral mode. For each initial height, the

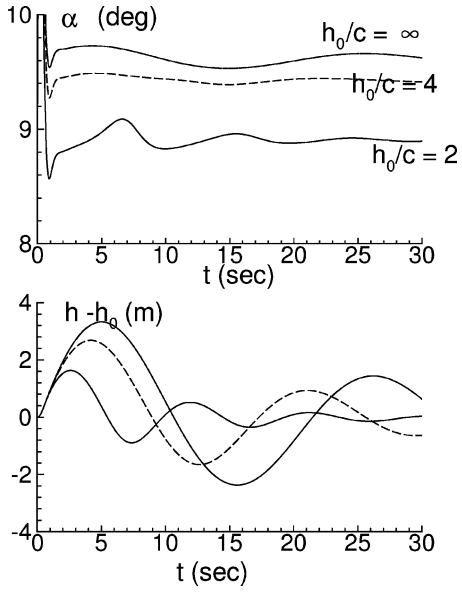

Fig. 14 Time history of the perturbed longitudinal motion beginning from different initial heights: ($\boldsymbol{H}\neq 0$).

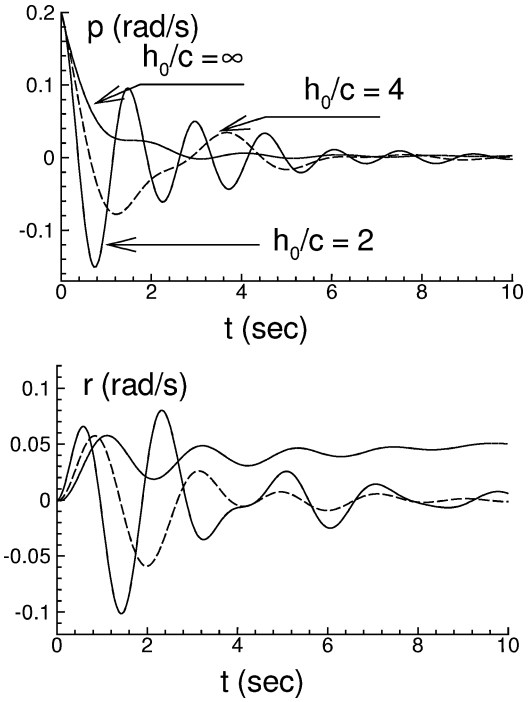

Fig. 15 Time history of the perturbed lateral motion beginning from different initial heights, ($H \neq 0$).

time histories show characteristic times that are in agreement with the data obtained through the eigenvalues analysis. For $h_0/c = 4$, the oscillating rolling mode is apparent together with the Dutch roll, while both rolling convergence and spiral modes disappear. At $h_0/c = 2$, the Dutch roll is obscured by the oscillating rolling, which produces the main effect. This result can be also obtained by analyzing the eigenvectors of each mode.

Conclusions

In this study the dynamics in ground effect is investigated accounting for the influence of the attitude on the vehicle dynamics. The Lagrange equations method applied to lifting bodies is used to express the forces and moments that are developed in ground effect. This method has general validity and contains the important elements for describing ground effect. In particular the method leads to the determination of aerodynamic force and moment coefficients in terms of roll, pitch, and flight-path angles. Comparisons between existing data in the literature and those obtained with the present method show that the procedure provides accurate results for aerodynamic force and moment of wings in steady and unsteady ground effect. Once the method is validated, the aerodynamic coefficients of a vehicle geometry are examined. The attitude effects on the vehicle aerodynamics are identified, and the unsteadiness induced by nonzero sink rates is explained. The trim calculation for the banked turn clarifies the behavior observed in ground effect, whereas the stability analysis yields explanations about the flying qualities with particular reference to the spiral mode stabilization and to the existence of the oscillating rolling. The nonlinear analysis, which is obtained by integrating the full set of the equations of motion, gives results in accordance with those obtained by means of the linear stability.

Acknowledgment

This work is partially supported by Italian Ministry of University.

References

[1]Staufenibel, R. W., and Schlichting, U. J., "Stability of Airplanes in Ground Effect," *Journal of Aircraft*, Vol. 25, No. 4, 1988, pp. 289–294.

[2]Walsh, D., and Cycon, J. P., "The Sikorsky Cypher UAV: A Multi-Purpose Platform with Demonstrated Missions Flexibility," *Proceedings of the Annual Helicopter Society 54th Annual Forum*, 1998, pp. 1410–1418.

[3]Lange, R. H., and Moore, J. W., "Large Wing-in-Ground Effect Transport Aircraft," *Journal of Aircraft*, Vol. 17, No. 4, 1979, pp. 260–266.

[4]Etkin, B., *Dynamics of Atmospheric Flight,* Wiley, New York, 1972, pp. 104–152, 259, 260.

[5]Kornev, N., and Matveev, K., "Complex Numerical Modeling of Dynamics a Crashes of Wing-in-Ground Vehicle," AIAA Paper 2003-600, Jan. 2003.

[6]Yang, Hee Joon, "A Study on the Enhancement of Lateral Motion of a Wing-in-Ground Effect Ship," M.S. Thesis, Dept. of Naval Architecture and Ocean Engineering, Seoul National University, Republic of Korea, Feb. 1999.

[7]Chung, Chang, R., and Muirhead, V. U., "Effect of Sink Rate on Ground Effect of Low-Aspect-Ratio Wings," *Journal of Aircraft*, Vol. 24, No. 3, 1987, pp. 176–180.

[8]Nuhait, A. O., and Mook, D. T., "Numerical Simulation of Wings in Steady and Unsteady Ground Effects," *Journal of Aircraft*, Vol. 26, No. 12, 1989, pp. 1081–1089.

[9]Nuhait, A. O., and Zedan, M. F., "Numerical Simulation of Unsteady Flow Induced by a Flat Plate Moving Near Ground," *Journal of Aircraft*, Vol. 30, No. 5, 1993, pp. 611–617.

[10]Han, C., Yoon, Y., and Cho, J., "Unsteady Aerodynamic Analysis of Tandem Flat Plates in Ground Effect," *Journal of Aircraft*, Vol. 39, No. 6, 2002, pp. 1028–1034.

[11]Rozhdestvensky, K. V., *Aerodynamics of a Lifting System in Extreme Ground Effect*, Springer-Verlag, Berlin, 2000, pp. 263–318.

[12]Kumar, P. E., "Some Stability Problems of Ground Effect Vehicle in Forward Motion," *Aeronautical Quarterly*, Vol. 18, Feb. 1972, pp. 41–52.

[13]Staufenbiel, R., "Some Nonlinear Effect in Stability and Control of Wing-in-Ground Effect Vehicles," *Journal of Aircraft*, Vol. 15, No. 8, 1978, pp. 541–544.

[14]Tuck, E. O., "Nonlinear Extreme Ground Effect on Thin Wings of Arbitrary Aspect Ratio," *Journal of Fluid Mechanics*, Vol. 136, 1983, pp. 73–84.

[15]Tuck, E. O., "Nonlinear Unsteady One-Dimensional Theory for Wing in Extreme Ground Effect," *Journal of Fluid Mechanics*, Vol. 98, 1980, pp. 33–47.

[16]Newman, J. N., "Analysis of Small-Aspect-Ratio Lifting Surfaces in Ground Effect," *Journal of Fluid Mechanics*, Vol. 117, 1982, pp. 305–314.

[17]Lamb, H., "On the Motion of Solids Through a Liquid," *Hydrodynamics*, 6th ed., Dover Publ., New York, 1945, pp. 160–201.

[18]de Divitiis, N., "Effect of Microlift Force on the Performance of Ultralight Aircraft," *Journal of Aircraft*, Vol. 39, No. 2, 2002, pp. 318–325.

[19]Lippisch, A. M., "Der 'Aerodynamische Bodeneffekt' und die Entwicklung des Flugflächen-(Aerofoil-)Bootes," *Luftfahrttechnik Raumfahrttechnik*, Vol. 10, Oct. 1964, pp. 261–269.

[20]VSAERO User's Manual, Rev. E5, Analytical Methods, Inc., Seattle, WA, April 1994, pp. 1–52.